SAND2017-3261C

SOLUTION MINING RESEARCH INSTITUTE
105 Apple Valley Circle
Clarks Summit, PA 18411, USA

Telephone: +1 570-585-8092
www.solutionmining.org

Technical Conference Paper

Potential Influence of Granular Salt on Cavern Stability

Brandon Lampe[1,2], John Stormont[2], Tim Lynn[2], Stephen Bauer[3]

[1]WSPIParsons Brinckerhoff, Houston, TX, USA
[2]University of New Mexico, Albuquerque, NM, USA
[3]Sandia National Laboratories, Albuquerque, NM, USA

SMRI Spring 2017 Technical Conference
24 – 25 April 2017
Albuquerque, New Mexico, USA

Solution Mining Research Institute Spring 2017 Technical Conference

Albuquerque, New Mexico, USA, 24-25 April 2017

Potential Influence of Granular Salt on Cavern Stability

Brandon Lampe[1,2], John Stormont[2], Tim Lynn[2], and Stephen Bauer[3]

[1]WSP|Parsons Brinckerhoff, Houston, TX, USA
[2]University of New Mexico, Albuquerque, NM, USA
[3]Sandia National Laboratories, Albuquerque, NM, USA

Abstract

Legislation, in the state of Louisiana, has recently modified regulations on the required minimum separation distance between a solution-mined cavern and the periphery of the host salt. In consideration of this, discussion and laboratory experiments will be presented here to provide insight into how the accumulation and consolidation of granular salt on the floor of a cavern may influence the floor stability and minimum separation distance. A summary of recent deformation and flow experiments on crushed salt are presented. These experiments were performed in an effort to quantify both the consolidation and transport properties of crushed salt under a combination of confining and pore pressures at elevated temperatures. During hydrostatic creep tests, volumetric strains were measured in excess of 20% that resulted from large decreases in pore volume. Additionally, gas flow measurements were made during creep consolidation, and results from tests show the permeability of crushed salt approaches that of intact salt during hydrostatic consolidation.

Key words: Granular Salt, Permeability, Salt Periphery

1 Introduction

Deformation of granular (or crushed) salt has been of interest to the dry mining and waste repository industries for decades because crushed salt can be economically used as a backfill and sealing material in these environments. In solution-mined caverns, granular salt (along with insoluble minerals) is often present in substantial quantities on the floor of a cavern; however, the potential for increased floor stability resulting from the deposition and consolidation of granular salt in a solution-mined cavern has been largely overlooked. Because granular salt is understood to consolidate with time until its constitutive properties are similar to intact salt, the geometry of a storage cavern floor may be understood to evolve as the granular salt covering the floor sufficiently consolidates to a state of intact salt.

A scenario resulting in the bulk deposition of granular salt on the floor of a cavern is a localized wall or roof failure. Localized failures in caverns are not uncommon and occur as a result of large stress concentrations tangential to cavern walls. A well documented case of a large wall failure was presented by Munson et al. (2000). As a result of these types of failures, a substantial volume of granular salt may accumulate on a cavern's floor, as depicted in Figure 1. As this process occurs, the walls become more stable and localized failures occur less frequently as the cavern shape is more spherical and local stress concentrations are reduced.

Recent legislation, regarding solution-mined caverns in U.S. state of Louisiana, has modified the minimum separation distance between subsurface caverns and the periphery of the host salt stock. In light of

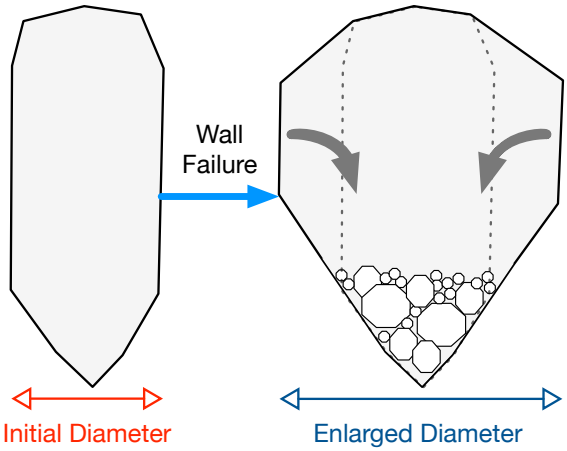

Figure 1: Illustration of how localized wall failures may enlarge the diameter of a solution-mined cavern and deposit granular salt on the floor of a cavern.

this, a question has been raised regarding how the accumulation and subsequent consolidation of granular salt on a cavern floor affects the floor stability along with the separation distance between adjacent caverns and the separation distance between a cavern and the edge of the host salt. Figure 2 illustrates a hypothetical scenario where a solution-mined cavern has been developed near an overhang structure in the host salt (Part A), and as granular salt accumulates on the cavern floor the wall separation distance between the edge of the host salt and the open cavern wall is increased (Part B). Does this increased separation distance result in an associated increase of hydraulic containment properties, e.g., reduced likelihood for a loss of cavern integrity?

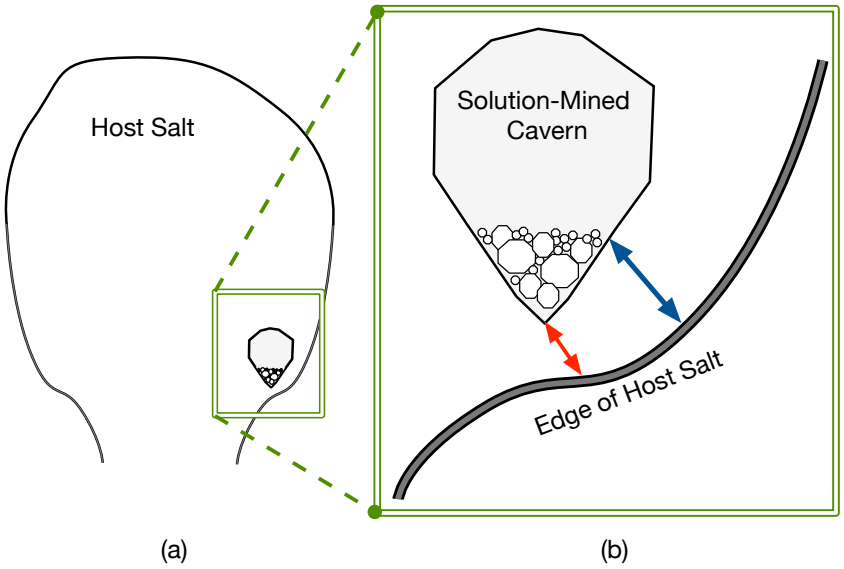

Figure 2: Potential influence of granular salt on the separation distance between a cavern wall and host salt periphery (a), where an initial separation distance (red arrow) is appreciably less than the separation distance after granular salt has accumulated (blue arrow) on the cavern floor (b).

In this study, the deformation and permeability of crushed salt has been experimentally evaluated at elevated temperatures under a combination of confining (P_c) and pore (P_p) pressures. Results presented herein focus on how pore pressure influences the deformation of crushed salt and how its permeability

evolves as it consolidates. These characteristics have been chosen because they may play a significant role in determining if the accumulation of granular salt on the floor of a cavern impacts a caverns stability.

2 Materials and Methods

Samples of crushed salt were prepared and tested under hydrostatic creep conditions where both a P_c and P_p were applied. Additionally, gas-permeability measurements were made during the creep stages of these tests. The following sections provide a description of the sample material and an overview of how they were prepared for testing. Following this, a description of the testing apparatus employed to performed the creep and permeability tests is presented.

2.1 Sample Description and Preparation

Test samples consisted of "mine-run" salt that had been excavated from the Salado formation at the Waste Isolation Pilot Plant (WIPP) facility near Carlsbad, NM or from Cargill's salt mine on the Avery Island salt dome in Louisiana. Mine-run salt was sieved such that the maximum particle diameter did not exceed 9.5 mm. After sieving, samples were oven dried at 110^oC for over 24 hours.

Each sample had an initial undeformed geometry of a right-circular cylinder and was jacketed by thin copper foil inside of a soldered lead tube. The undeformed lead tube had an approximate length of 23 cm (9 in) with an internal diameter of 10 cm (4 in). These copper and lead jackets covered the vertical sides of the sample and at the open ends of these jackets, steel end caps with a diameter of 10 cm (4 in) and height of 5 cm (2 in) were used to hold the crushed salt in place. A similar approach for jacketing was used by Broome et al. (2015), and a more detailed description the jacketing approach is provided in their paper.

The undeformed samples had a porosity ranging from 30 to 40% and the bulk volume of crushed salt was approximately one liter. Figure 3 includes an image of an undeformed sample in part (a). After each sample was assembled, it was placed inside the testing apparatus and preconditioned.

(a) Undeformed (b) Preconditioned (c) Post Creep

Figure 3: Pictures of a typical sample a the three different stages, (a) undeformed prior to the application of pressure, (b) preconditioned by being rapidly loaded to 20 MPa and unloaded under drained conditions, and (c) post creep test.

Samples were preconditioned to aid in the accuracy of measuring deformations during the creep tests, this was completed in a fashion similar to Brodsky (1994, pg. 31). Initial tests performed without pre-

conditioning resulted in (1) nonuniform radial deformations (2) poor quantification of the initial bulk sample volume, and (3) excessive volume deformations that could not be measured by external deformation gages.

The process of preconditioning consisted of loading the sample, in drained conditions, with a P_c at a rate of 4 MPa/min up to 20 MPa and then immediately unloading the sample back down to atmospheric conditions. The sample was loaded at ambient temperature without the use of external gages. After the preconditioning had been completed, measurements of mass and volume were made to determine the bulk density of the crushed salt. Volume measurements were made using two different techniques: (1) calipers were used to measure the external dimensions of the sample and (2) fluid displaced by the sample when immersed in a calibrated fluid-filled tank. Both of these techniques relied on prior measurements of all the non-salt components that made up the sample (lead and copper jackets, end caps, etc.). Results from these two methods were generally in good agreement. Figure 3 includes an image of the preconditioned sample (prior to creep) in part (b).

Sample porosity was determined by relating the bulk sample density (ρ) to the reference values for density (ρ_{ref}) of in situ rock salt at WIPP and Avery Island, 2160 and 2140 kg/m^3 , respectively, to the intact connected porosity of zero (Brodsky et al., 1996). Based on these reference values, the ratio of the current interconnected pore volume (V_p) to the current bulk sample volume (V) is termed the bulk sample porosity (ϕ), Eqn. 1.

$$\phi = \frac{V_p}{V} = 1 - \frac{\rho}{\rho_{ref}} \tag{1}$$

2.2 Testing Apparatus

Experiments were performed in a pressure vessel equipped with multiple ports that were used to suspend the sample, flow test fluids, and run wires for data acquisition. Figure 4a provides a general overview of the testing apparatus. P_c was supplied by the application of silicone oil on the exterior of the lead jacket, and the flow of silicone oil was controlled by a Teledyne Isco D Series Syringe Pump. P_p was supplied via an external reservoir of pressurized gas that was manually regulated. Ring heaters mounted on the exterior of the pressure vessel were used to supply heat to the sample, and the confining fluid temperature was regulated using measurements from a thermocouple immersed in the confining fluid.

Deformations during the creep tests were measured using two different methods, (1) metering the confining fluid with the syringe pump and (2) a pair of lateral deformation gages mounted on the exterior of the lead jacket, shown in Figure 4b. The use of lateral deformation gages was prompted by the extreme sensitivity of confining fluid volume to subtle changes of temperature in the laboratory environment. The lateral deformations gages were constructed from a metal ring with four high-temperature strain gages adhered to it in a configuration similar to that described by Schuler (1978). The lateral deformation gages had a working range of 1.25 cm (0.5 in) and were shown to provide consistent measurements at temperatures up to 250^oC.

The use of two fundamentally different methods (metering fluid and measuring sample diameter) for determination of the transient sample volume allowed for validating the assumptions of isotropic and homogeneous deformation during the tests. That is, volumetric deformations were calculated based on a change in sample diameter measured between two sets of points on the exterior of the sample, and from these deformations, changes in the bulk sample volume were calculated (with the assumptions of isotropy and homogeneity). The calculated bulk sample volume changes as determined by the two sets of external deformation gages were then compared to each other and to the metered change in confining fluid volume under constant pressure and temperature conditions. Results from all three independent sets of measurements agreed well.

2.3 Creep Test Procedure

After each sample had been preconditioned and an initial bulk density had been determined, the sample was placed back into the pressure vessel and heated to the desired temperature. Sample heating was performed with the sample completely submerged in the confining fluid. The upper bleed valve remained

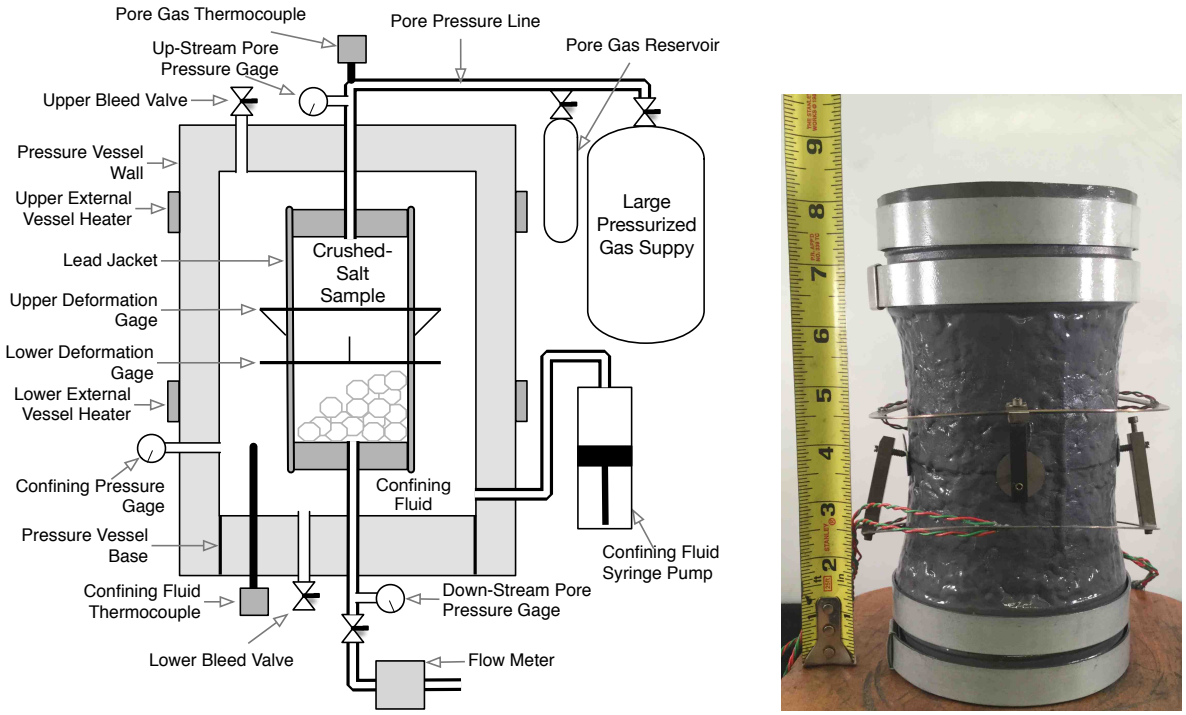

(a) Generalized schematic of the testing apparatus (not to scale).

(b) Deformation gages on deformed sample.

Figure 4: Illustrations of the experimental setup used for creep and permeability testing of crushed salt.

open to the atmosphere during heating, which allowed for the confining fluid to be expelled from the pressure vessel as it expanded during the heating process and for the confining fluid to remain unpressurized.

Once the confining fluid had reached a stable temperature of 170^oC for over 12 hours, the pressure vessel was closed in. Fluid pressures were increased at a rate of 4 MPa/min until the desired creep test pressures were achieved. Deformations during the pressure increase were observed to be both elastic and plastic; however, only the creep deformations during constant pressure conditions are considered here.

For clarity, P_c refers to the macroscopic fluid pressure applied to the outer surface of the sample. P_p refers to the macroscopic gas pressure in the interconnected pore volume of the bulk sample, and P_d is the difference between P_c and P_p. During the pressure increase, P_c and P_p were independently controlled such that P_c was increased until the desired value of P_d was achieved. Then, P_c and P_p were increased uniformly (holding P_d constant) until the desired pressures for the creep tests were achieved. A summary of selected creep tests are presented in Table 1. The porosity measurements following the preconditioning (ϕ_{pc}) of each sample (via caliper and fluid immersion) are presented in Table 1 along with the porosity values measured at the start of the creep test (ϕ^0_{crp}), after the increase of pressure. Creep tests considered here were all performed on crushed salt from the WIPP.

Table 1: Summary of creep test conditions.

Test/Sample Label	P_c MPa/psi	P_p MPa/psi	P_d MPa/psi	ϕ_{pc} %	ϕ^0_{crp} %
A	30/4350	0/0	30/4350	21.8	10.9
B	30/4350	10/1450	20/2900	21.3	11.8
C	30/4350	20/2900	10/1450	21.0	17.8

2.4 Permeability Measurement Procedure

Permeability measurements were performed on crushed salt from the WIPP (W) and Avery Island (A) facilities, and a summary of the test conditions are presented in Table 2. The creep tests here were performed in a manner similar to those described in the previous section, with the exception that these tests were performed under drained conditions (constant $P_p = 0$). At periodic intervals during these creep tests, permeability measurements were performed with nitrogen or helium gas, where the P_p was negligible with respect to P_c ($P_p \ll P_c$).

Table 2: Summary of permeability test conditions.

Test/Sample Label	Confining Pressure (P_c) MPa/psi	Temperature $^oC/^oF$	Test Duration Days	Final Porosity
W1	20/2900 to 38/5500	90/195	12	0.033
W2	20/2900	250/480	13	0.006
W3	20/2900	90/195	112	0.083
A1	20/2900	250/480	8	0.011
W4	20/2900	175/350	3	0.056
W5	20/2900	175/350	3	0.019
W6	40/5800	90/195	10	0.030

As samples experienced continued volumetric deformation deformation under hydrostatic creep conditions, the pore volume and associated permeability decreased appreciably. Permeability values (k) were interpreted from measured flow rates (q) at standard temperature (T_{std}) and pressure (P_{std}) using Darcy's law for compressible flow, as shown in Equation 2.

$$k = \frac{2q\mu L}{A}\left(\frac{P_{std}}{P_{up}^2 - P_{dwn}^2}\right) \tag{2}$$

Where the flow path is assumed to be represented by the sample length (L) over the cross-sectional area (A), and the flow is driven by the gradient between the upstream (P_{up}) and downstream (P_{dwn}) pressures. Because the flow measurements were made while the sample was at an elevated temperature, the permeability measurements accounted for the temperature dependency of gas viscosity (μ). Additionally, because gas flow in low-permeability media can be affected by interaction between the gas molecules and the flow path, a correction for gas-slip (or Klinkenberg correction) was also applied to the interpreted data (Klinkenberg et al., 1941).

Permeability values for the crushed salt ranged by over over six orders of magnitude for some samples, which necessitated the use of multiple measurement and interpretation techniques. When the measured permeability was greater than $5 \cdot 10^{-16}$ m^2, steady-state flow tests were employed, where the gas flow rate ranged from 20 standard liters per minute (SLM) down to one standard cubic centimeter per minute (SCCM). For permeability values ranging from $1 \cdot 10^{-15}$ to $5 \cdot 10^{-19}$ m^2, a quasi-steady method was employed (Jannot and Lasseux, 2012). And when the permeability was below $5 \cdot 10^{-19}$, flow measurements were made using a mass spectrometer with helium gas, as described by Bauer et al. (2015).

3 Results

Results here will be broken down into two categories that are believed to be of importance to the solution-mining industry, (1) the influence of pore pressure on the deformation of crushed salt during hydrostatic creep and (2) the evolution of crushed-salt permeability with porosity.

Table 3: Comparison of porosity (ϕ) at a constant plastic volumetric strain rate $(\dot{e}_v)$ from Figure 5b along with the pressure difference (P_d).

Test/Sample Label	ϕ %	$\dot{e}_v^p$ sec^{-1}	P_d MPa
A	9.1	10^{-6}	30
B	10.7	10^{-6}	20
C	16.4	10^{-6}	10

3.1 Creep Test Results

Deformations presented below were all observed during a state of constant P_c and P_p, and following the tests, when the samples were unloaded, these deformations have remained indefinitely; therefore, all deformations described in this paper are considered plastic. Deformation of the samples are quantified in terms of a scalar metric describing the bulk volume change of the sample. This metric is the plastic volumetric strain (e_v^p), which is considered positive in compression (decreasing volume) and defined in terms of the natural logarithm as shown in Eqn. 3, where V and V^0 represent the current and preconditioned bulk sample volumes, respectively. The plastic volumetric strain rate $(\dot{e}_v^p)$ is primarily considered in this paper, and it is defined as the ratio of incremental plastic change in volume strain (Δe_v^p) to the incremental change in time (Δt), Eqn. 4.

$$e_v^p = -ln\left(\frac{V}{V^0}\right) \tag{3}$$

$$\dot{e}_v^p = \frac{\Delta e_v^p}{\Delta t} \tag{4}$$

The creep test results presented here are focused on identifying the role of P_p on the $\dot{e}_v^p$; therefore, a substantial effort was taken to keep other parameters that influence the test results constant. That is, the water content, particle size distribution, temperature, and P_c were nearly constant between all tests and their respective influences will not be considered here.

Figure 5a illustrates the change of ϕ as the samples reconsolidate with test duration for each of the three creep tests. These results all display a similar trend of decreasing ϕ over the creep test duration. Figure 5b provides direct the comparison of the $\dot{e}_v^p$ as a function of ϕ, where P_c equals 30 MPa for all tests while the P_p is different for each. These results show a trend that is not consistent with the understanding that $\dot{e}_v^p$ depends only on ϕ and P_c. Table 3 considers these three tests when their respective $\dot{e}_v^p$ is 10^{-6} sec^{-1}. Here, samples with a wide range of ϕ all exhibit a similar $\dot{e}_v^p$, e.g., the three samples ϕ values vary by over 7%, but they all exhibit a similar $\dot{e}_v^p$. This observation indicates the plastic deformation of crushed salt under hydrostatic creep conditions is influenced by the P_p. For an alternative view, consider the $\dot{e}_v^p$ of Samples A and B when they are both at a ϕ of 10% in Figure 5b; their values of $\dot{e}_v^p$ differ by over an order of magnitude, where Sample A (under a P_d of 30 MPa) is deforming at a rate much greater than Sample B (under a P_d of 20 MPa).

Results presented here indicate the $\dot{e}_v^p$ is influenced by both the ϕ and P_d. This observation is understood here to result from a non-hydrostatic state of stress within the salt particles, which implies shear stress exists over a representative elementary volume (REV) while the bulk sample is subjected to a purely hydrostatic state of stress. The shear stress experienced over the REV is recognized to cause permanent shear deformation, e.g., that described by a maximum distortional energy (Mises) type yield criterion. Deformation of the salt particles is understood to result in a reduced pore volume, which results in a reduced bulk volume during a hydrostatic creep test. The experimentally observed influence of the P_d on the creep deformation rate illustrates how P_p affects the shear deformation of porous materials under a bulk hydrostatic stress, unlike the response observed in materials which have no interconnected pore space and are relatively insensitive to P_p.

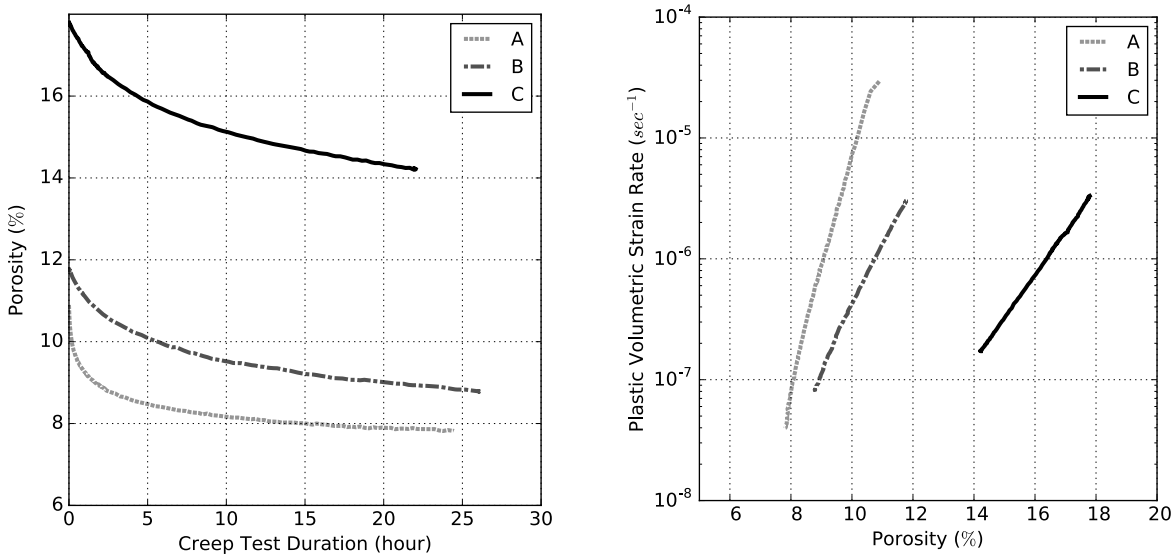

(a) Porosity versus creep test duration.

(b) Volumetric strain rate versus sample porosity.

Figure 5: Illustrations of the experimental setup used for creep and permeability testing of crushed salt.

3.2 Permeability Measurement Results

Because the accumulated salt on the floor of a solution-mined cavern is likely to have properties ranging between dilated salt and crushed salt, both types of salt are considered here. Figure 6 presents the measured permeability versus porosity for the crushed-salt samples listed in Table 2 (red) along with permeability values of dilated WIPP salt (black) and a general range of values for intact salt (shaded blue). Experiments performed on dilated WIPP salt permeabilities were completed by Stormont and Daemen (1992), and Popp et al. (2001) further developed the permeability-porosity relationship for these data. Results from both data sets show general trends of decreasing permeability with decreasing porosity, and as the porosity of both dilated and crushed salt approaches that of intact salt so does their respective permeability. However, crushed-salt consistently exhibits a lower permeability while at the same porosity as dilated salt.

In an effort to conceptualize our understanding of the data presented in Figure 6, a schematic illustrating the generalized evolution of both crushed salt and dilated salt under hydrostatic creep conditions is presented in Figure 7, which depicts the transition from an initial state at the start of a creep test to the final state similar to that of intact salt. In the *Initial State*, the fundamental difference between crushed and dilated salt is illustrated by the arrangement of their respective particles. These different particle arrangements result in markedly different porosity values while having similar permeability. Particle boundaries within a sample of crushed salt are not aligned and allow for a substantial volume of interconnected porosity, whereas the particle boundaries of dilated salt remain aligned and allow for only a small increase in porosity relative to intact salt.

The *Intermediate State*, in Figure 7, presents both crushed and dilated salt after some duration of hydrostatic creep have occurred and the porosity of both have been reduced. The respective images show how crushed and dilated salt undergo a fundamentally different type of deformation while both under a macroscopic hydrostatic stress. Crushed-salt particles change shape as they deform into and fill the pore space; this deformation is understood to be described by maximum distortional energy or Mises type yield criteria. However, dilated-salt particles are understood to maintain their shape and simply slide along particle boundaries; where this type of plastic deformation is understood to be governed by the frictional resistance to sliding between particles. Therefore, dilated salt may be understood to yield according to a Mohr-Coulomb type criteria, which depends on both normal and shear stresses. Because of these fundamental differences in deformation, under similar stress conditions dilated salt will exhibit a reduced porosity and associated permeability similar to intact salt in a matter of hours or days, whereas the deformation of

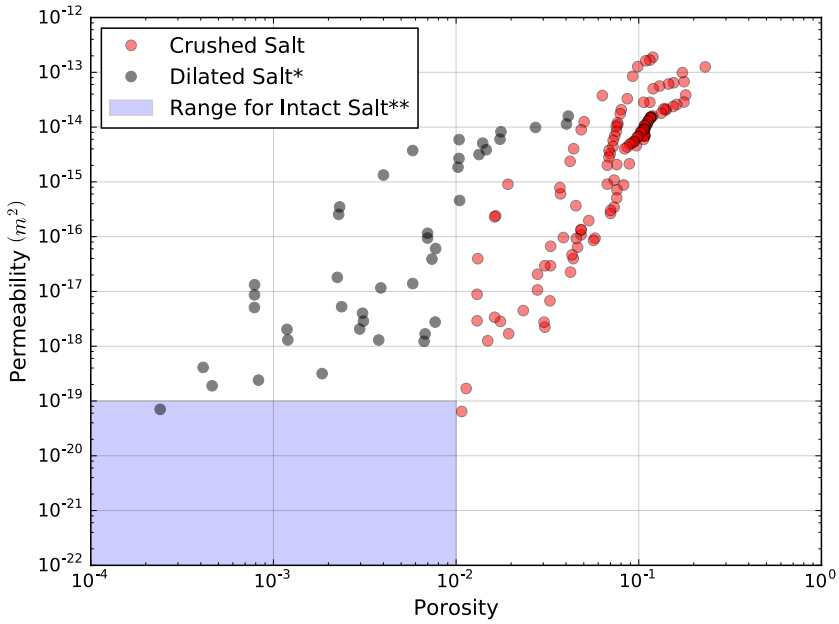

Figure 6: Permeability versus porosity under hydrostatic stress for crushed salt, dilated intact salt and a range intact salt; where dilated intact salt data (*) is from Stormont and Daemen (1992) and the range of intact salt data (**) has been compiled from multiple sources (McTigue, 1986; Amro et al., 2012; Sutherland and Cave, 1980; Bérest et al., 2001)

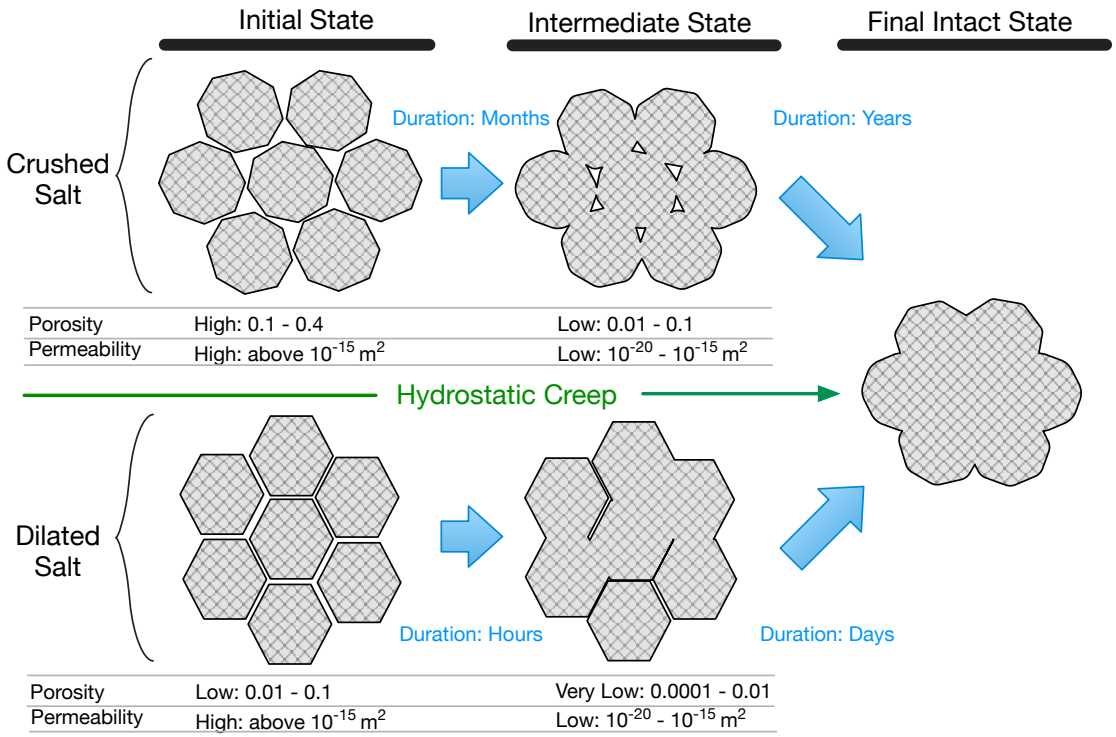

Figure 7: Genearlized comparison of pore structure, porosity and permeability between crushed and dilated salt as they transition to intact salt under a hydrostatic confining pressure of nominally 20 MPa at an ambient temperature in a dry environment.

crushed salt particles and subsequent reductions of porosity and permeability necessitate a substantially greater duration. However, after sufficient time, both crushed and dilated salt are understood to reach a final porosity and permeability similar to that of intact salt, as depicted in the *Final Intact State* of Figure 7.

4 Conclusion

Deformation and permeability of crushed salt have been experimentally evaluated at elevated temperatures under a combination of confining (P_c) and pore (P_p) pressures. The experimentally observed influence of the P_d on the creep deformation rate illustrates how P_p mitigates the shear deformation of crushed salt under a bulk hydrostatic stress, unlike the response observed in materials which have no interconnected pore space and are relatively insensitive to P_p. This characteristic may inhibit the ability of crushed salt to consolidate on the floor of salt cavern while exposed to a substantial gas or brine pore pressure, but the influence of brine on consolidation was not considered here. Spiers and Brzesowsky (1993) have previously shown the presence of brine (even saturated brine) increases the consolidation rate of crushed salt; however, they did not consider the influence of brine pressure on shear stress within the salt particles. Therefore, further analysis is needed to understand how or if crushed salt would appreciably consolidate in a solution-mined cavern environment.

Experimental results presented here have shown that both crushed and dilated salt have a permeability similar to intact salt when their respective porosity approaches that of intact salt. Based on these experimental results, if salt accumulated on the floor of a solution-mined cavern were consolidated to a sufficiently low porosity, the accumulated salt would have the permeability and associated sealing ability of intact salt.

Acknowledgement

This material is based upon work supported by the U.S. Department of Energy (DOE) Nuclear Energy University Program (NEUP) Grant Number DE-NE0000733. Sandia National Laboratories is a multi-mission laboratory managed and operated by Sandia Corporation, a wholly owned subsidiary of Lockheed Martin Corporation, for the U.S. Department of Energy's National Nuclear Security Administration under contract DE-AC04-94AL85000.

References

M. Amro, F. Häfner, and C. Freese. Modern in situ and laboratory measurements of permeability and porosity to prove tightness of underground storage of hydrogen, natural gas, and co2. SMRI Technical Conference Paper, Fall Conference, Bremen, Germany, 2012.

S.J. Bauer, M.Y. Lee, W.P. Gardner, et al. Helium-mass-spectrometry-permeameter for the measurement of permeability of low permeability rock with application to triaxial deformation conditions. In *49th US Rock Mechanics/Geomechanics Symposium*. American Rock Mechanics Association, 2015.

P. Bérest, V. de Greef, and B. Brouard. The influence of permeability and stress on spherical hollow salt samples. In *Salt Permeability Testing*, number 2001-8 in SMRI Research Project, October, 2001.

N. S. Brodsky. Hydrostatic and shear consolidation tests with permeability measurements on waste isolation pilot plant crushed salt. Contractor Report by RE/SPEC inc. SAND 93-7058, 1994.

N.S. Brodsky, F.D. Hansen, and T.W. Pfeifle. Properties of dynamically compacted waste isolation pilot plant salt. In Henry Reginald Hardy Michel Aubertin, editor, *Mechanical Behaviour of Salt: 4th Conference*, number SAND96-0838C. Trans Tech, 1996.

S.T. Broome, S.J. Bauer, F.D. Hansen, and M.M. Mills. Mechanical response and microprocesses of reconsolidating crushed salt at elevated temperature. *Rock Mechanics and Rock Engineering*, 48(6):2615–2629, 2015.

Yves Jannot and Didier Lasseux. A new quasi-steady method to measure gas permeability of weakly permeable porous media. *Review of Scientific Instruments*, 83(1):015113, 2012.

L.J. Klinkenberg et al. The permeability of porous media to liquids and gases. In *Drilling and production practice*. American Petroleum Institute, 1941.

D.F. McTigue. Thermoelastic response of fluid-saturated porous rock. *Journal of Geophysical Research: Solid Earth*, 91(B9):9533–9542, 1986.

D.E. Munson, S.J. Bauer, C.A. Rautman, B.L. Ehgartner, and A.R. Sattler. Analysis of the massive salt fall in big hill cavern 103. Sandia Report SAND2003-0703, Sandia National Laboratories, Albuquerque, New Mexico 87185, 2000.

T. Popp, H. Kern, and O. Schulze. Evolution of dilatancy and permeability in rock salt during hydrostatic compaction and triaxial deformation. *Journal of Geophysical Research: Solid Earth*, 106(B3):4061–4078, 2001. ISSN 2156-2202. doi: 10.1029/2000JB900381. URL http://dx.doi.org/10.1029/2000JB900381.

K. W. Schuler. Lateral-deformation gage for rock-mechanics testing. *Experimental Mechanics*, 18(12): 477–480, 1978.

C.J. Spiers and R.H. Brzesowsky. Densification behaviour of wet granular salt: Theory versus experiment. In *Seventh Symposium on Salt*, volume 1, pages 83–92. Elsevier Amsterdam, 1993.

J.C. Stormont and J.J.K. Daemen. Laboratory study of gas permeability changes in rock salt during deformation. In *International journal of rock mechanics and mining sciences & geomechanics abstracts*, volume 29, pages 325–342. Elsevier, 1992.

H.J. Sutherland and S.P. Cave. Argon gas permeability of new mexico rock salt under hydrostatic compression. *International journal of rock mechanics and mining sciences & geomechanics abstracts*, 17(5): 281–288, 1980.